Multiplexing onto a spatial light modulator using random binary patterns

Jeffrey A. Davis,[a] Ignacio Moreno [b,c,*] Shang Gao [b]
María del Mar Sánchez-López [b,d] and Don M. Cottrell[a]

[a]San Diego State University, Department of Physics, San Diego, California, United States
[b]Universidad Miguel Hernández de Elche, Instituto de Bioingeniería, Elche, Spain
[c]Universidad Miguel Hernández de Elche, Departamento de Ciencia de Materiales, Óptica y Tecnología Electrónica, Elche, Spain
[d]Universidad Miguel Hernández de Elche, Departamento de Física Aplicada, Elche, Spain

ABSTRACT. We introduce an approach for encoding a variety of independent outputs from a computer-generated diffractive optical element displayed on a spatial light modulator (SLM). In this approach, random binary 0-1 orthogonal patterns are multiplied to the different phase functions, effectively multiplexing the corresponding different outputs. We show experimental results with different examples of multiplexed phase functions. Additional functions can be multiplexed simply by adding more random binary patterns. We demonstrate the generation of up to eight different independent outputs. Although the technique was demonstrated years ago, nowadays it can be applied with high-resolution SLMs with a very large number of pixels, thus allowing for a larger number of multiplexed functions without significant degradation. Nevertheless, high-resolution SLMs are affected by pixel crosstalk caused by the fringing field effect. We show that the random patterns are quite sensitive to this effect, leading to a significant undesired DC order. Two alternative strategies to avoid this degradation and make the random multiplexing technique efficient are discussed.

1 Introduction

The concept of multiplexing involves the capability of generating multiple output beams from a given input pattern. Here we address the problem of multiplexing diffractive functions onto a hologram or a spatial light modulator (SLM). When multiplexed, the different patterns might interfere with each other, causing a degradation of the individual outputs. Thus methods to reduce this degradation are necessary. If we simply add the patterns, the process is nonlinear.[1,2] Alternatively, the diffractive elements can be divided into different areas and the pattern can be encoded for each output on a different area.[1] However, this reduces the spatial width of each pattern and implies a loss of resolution.

Multiplexing phase functions have been applied in the past to achieve multifocus lenses[2] and increase the depth of focus,[3] to create multiple optical traps in microscopy,[4] or in optical communications to implement systems based on orbital angular momentum[5] or more general spatial mode division multiplexing techniques.[6] In all cases, it is interesting to be able to multiplex as many elements as possible with the minimum crosstalk.[7,8]

---

*Address all correspondence to Ignacio Moreno, i.moreno@umh.es

In this work, we apply an approach for easily creating a variety of output beams that are individually independent. Although this approach can be implemented using a static hologram or a computer-generated diffractive optical element, we concentrate on using a programmable SLM. The approach is based on a random selection at each pixel of the phase level of the multiplexed diffractive element. It was developed originally with very low-resolution devices[1,9] and applied to multiplex diffractive lenses[9] and phase-only filters for pattern recognition in the Fourier and the Fresnel domains.[10] More recently, similar approaches have been used to achieve multiple-beam optical phase arrays[11] or to design holograms generating composite vortex beams.[12]

Nowadays, liquid crystal displays (LCDs) are a mature and widely used SLM technology. Liquid-crystal SLMs can be operated as continuous phase-only or binary-phase-only SLMs.[13] Modern high-resolution devices have a very large number of pixels with a small size, and liquid-crystal SLMs with 4K resolution and beyond are commercially available.[14] Therefore, the random multiplexing technique can be applied with a larger number of multiplexed diffractive patterns encoded simultaneously (note that initial works used SLMs with only 128×128 pixels).[2] However, these modern high-resolution liquid-crystal on silicon (LCOS) SLM devices are typically affected by pixel cross-talk caused by the fringing field effect.[15] The random multiplexing approach is very sensitive to this problem because it results in phase functions with sharp phase changes between adjacent pixels.

In this work, we demonstrate a system in which we multiplex the Fourier transforms of different desired outputs using the random approach. We show how the fringing field effect results in an undesired DC diffraction order caused by the randomness of the phase function. Then we show two simple approaches to reduce this effect: one based on increasing the SLM phase modulation range and one based on enlarging the size of the random dots. Once this effect is reduced, experimental results that demonstrate the capability for the random multiplexing approach to encode a variety of output beams are included.

This paper is organized as follows. After this introduction, Sec. 2 introduces the experimental system and shows initial experimental results that evidence the problem that arises from the fringing field effect in the SLM. Section 3 discusses the extension to allow for multiple outputs and shows experimental results on the effective generation of multiple beams. Finally, in Sec. 4, the conclusions of the work are presented.

2 Experimental System and Methods

Our experimental system is similar to that used earlier[16] (Fig. 1). An He–Ne laser is first spatially filtered and collimated with a converging lens (L_1). We employ an LCOS SLM device, which is currently the most common SLM technology.[13] Because these are reflective devices, the system must be adapted to a reflective geometry as in Fig. 1. The LCOS-SLM is a Hamamatsu device, model X10468-0, with 792×600 pixels, a pixel spacing of $\Delta = 20 \ \mu$m, and a parallel-aligned liquid-crystal configuration.
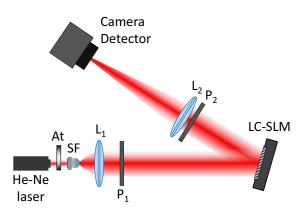

Fig. 1 Scheme of the optical setup. At, attenuator; SF, spatial filter; L, convergent lenses; P, linear polarizers; and LC-SLM, liquid-crystal spatial light modulator.
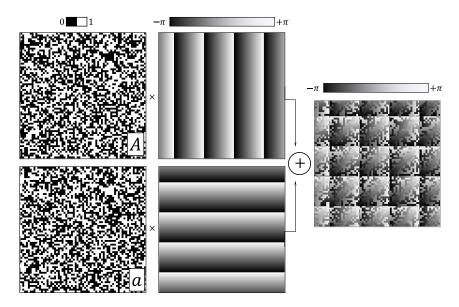
First, the SLM phase modulation was calibrated using a standard technique, valid for parallel aligned LCDs, where the input polarizer (P_1) was oriented at 45 deg with respect to the LC director and the reflected beam was analyzed with a linear analyzer (P_2) oriented parallel and crossed with respect to the input polarizer. A uniform gray level ($g \in [0,255]$) was addressed to the SLM, and the measured normalized intensity was fit to the crossed and parallel intensities, given by $i_\perp = \sin^2(\phi/2)$ and $i_\parallel = \cos^2(\phi/2)$, respectively, where ϕ is the retardance of the SLM. The SLM phase modulation versus the gray level is given by $\varphi(g) = \phi(g) - \phi_0$, where we select $\phi_0 \equiv \phi(g = 0)$ as the reference. We measured a phase modulation depth that exceeds 2π for the operating wavelength of 632.8 nm.[16]

To operate the SLM as a phase-only display, the input linear polarizer (P_1) is oriented with its transmission axis parallel to the director axis, so the beam can be fully phase modulated. The reflected beam is then focused on a camera detector by means of a second convergent lens (L_2), where the Fourier transform of the pattern displayed in the SLM can be captured. An attenuator (At) placed at the laser output is used to adjust the intensity level.

The multiplexing approach is illustrated in Fig. 2. We select image arrays of $N \times N$ pixels, with $N = 1024$, so they overfill the SLM screen in both directions when they are displayed. We first create a random binary amplitude pattern, in which each pixel is randomly given a value of $+1$ or 0. For convenience, we label this pattern as A. Figure 2 shows an expanded version with 128×128 pixels that illustrates the method. Next we generate the complementary pattern in which the pixel values are reversed. All pixels having a value $+1$ in the first pattern are now given 0, and vice versa. For convenience, we designate this array as a. In Fig. 2, black and white denote amplitude values 0 and 1 binary in the random patterns A and a, respectively. Each binary pattern is selected to have half of the pixels ($N^2/2$), and they fulfill $A(x, y) \cdot a(x, y) = 0$ and $A(x, y) + a(x, y) = 1$.

Now we encode two different phase diffractive functions onto each binary pattern. For that purpose, we simply multiply one phase function by the binary mask A and the other one by the complementary binary mask a. To illustrate the technique, we start by encoding one different blazed diffraction grating onto each pattern. Therefore, this simple multiplexed phase pattern $F(x, y)$ is written as

$$F(x, y) = A(x, y)e^{i\gamma x} + a(x, y)e^{-i\gamma y}. \tag{1}$$

Fig. 2 Design of the multiplexed phase function using the random approach. The left column shows the two complementary binary amplitude masks *A* and *a*. They multiply linear phases (central column) to produce two different outputs at different locations, here in horizontal and vertical directions. The corresponding results are added to provide the final multiplexed phase-only function.

The first blazed grating diffracts the output in the horizontal direction and is multiplied by the random binary pattern A. Then a second blazed grating that diffracts the output in the vertical direction is multiplied by the complementary random binary pattern a.
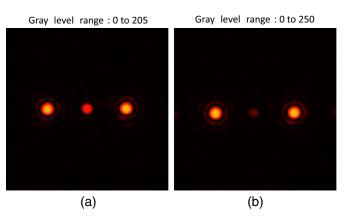
The phase function of these linear blazed gratings is shown in Fig. 2 in gray levels with phase range 2π. The multiplexed function $F(x, y)$ given by Eq. (1) is a phase-only function that can be displayed directly on the SLM. The maximum gray level is adjusted to match the 2π phase modulation for the operating wavelength. (In our SLM, this occurs for gray level 205 at the wavelength 632.8 nm.)[16]

Let us note that the simple addition of the two blazed gratings to produce the two outputs, $e^{i\gamma x} + e^{-i\gamma y}$, results in a complex-valued function that cannot be directly implemented in a phase-only SLM and requires additional techniques for encoding complex values. By contrast, the function $F(x, y)$ in Eq. (1) is a phase-only function. Therefore, it can be encoded directly onto the LCOS-SLM, with each pixel of the computer program corresponding to one pixel of the display. The desired outputs are formed in the focal plane of the lens and captured by the camera detector (Fig. 1).
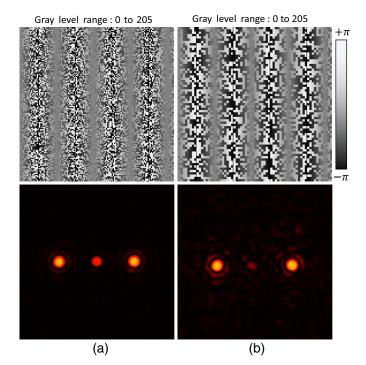
Figure 3(a) shows some first experimental results in which we use two blazed gratings diffracting horizontally in opposite directions. The output shows the two expected focused spots. However, a strong DC order is also present in the center. This is a result of the well-known fringing field effect present in LCOS-SLMs,[15] a pixel crosstalk that makes the phase nonuniform across the pixel. This effect increases as the voltage difference between neighbor pixel increases[16] and results in a DC term that is focused on axis in the Fourier transform plane.[17]

To calibrate the SLM phase modulation, we used a standard technique[16] in which uniform gray level images are addressed, i.e., the same voltage was applied to all pixels. Therefore, the fringing field effect was minimized. When a blazed grating is displayed in the SLM, the phase levels increase linearly as a function of position, but there are sharp 2π phase transitions every period. The fringing field effect strongly affects the pixels where abrupt transitions from maximum to minimum phase take place, effectively reducing the phase difference and therefore, contributing to the DC term. In addition, the random approach introduces rapid phase variations between many neighbor pixels, as shown in the final phase mask in Fig. 2. These rapid phase variations also contribute to the DC term in Fig. 3(a).

We discuss two possible methods of minimizing this unwanted DC order. The easiest way is to increase the phase depth of the SLM. In the result shown in Fig 3(a), we used a maximum gray level of 205 that corresponds to the 2π phase modulation measured in the calibration. In Fig. 3(b), the same pattern was displayed in the SLM, but we increased the maximum gray level to 250, which corresponds approximately to a 2.5π phase modulation measured in the calibration. This change does not affect the lower voltages required for the lower phases, but it increases the voltages required for higher phases. The fringing field effect reduces the slope of the ideal 2π phase jump.[18] Increasing the maximum value in the addressed gray level ramp pattern

Gray level range : 0 to 205 Gray level range : 0 to 250

(a) (b)

Fig. 3 Experimental results of multiplexing two opposite blazed gratings. (a) Result when the maximum gray level is adjusted to 2π phase modulation ($g = 205$). (b) Result when the maximum gray level is increased ($g = 250$) to enlarge the phase modulation depth.

Fig. 4 Experimental results of multiplexing two opposite blazed gratings. (a) Result with a random pattern with one pixel size. (b) Result with a random pattern with 2×2 macropixels. On top of each experimental capture, detail of the corresponding phase mask is shown.
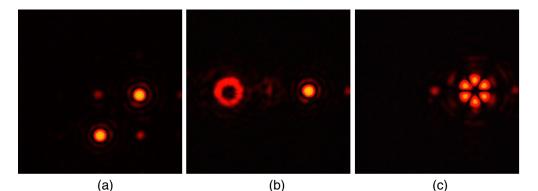
increases the slope of the phase jump and compensates the fringing field effect while satisfying the blazing requirements. As a result, the DC term is practically eliminated, as shown in Fig. 3(b).

In Fig. 4, we explored another approach to reduce the DC term caused by the fringing field effect. Here we keep the maximum gray level at $g = 205$ but change the size of the random dots used for the binary amplitude patterns. Instead of creating these patterns over the entire 1024×1024 array and assigning a different value to each pixel, we make the random pattern with larger "macropixels" consisting of multiple individual pixels. Figure 4(a) shows the case in which each random spot consists of a single pixel, showing a strong DC. In Fig. 4(b), we increased the random pattern macropixel size to be 2×2 pixels. This figure shows how the intensity of the DC term is reduced as well. The advantage of this approach is that it can be applied with SLMs that have a phase modulation range that does not exceed 2π. The disadvantage is that the effective number of random pixels is reduced, and the background noise increases.
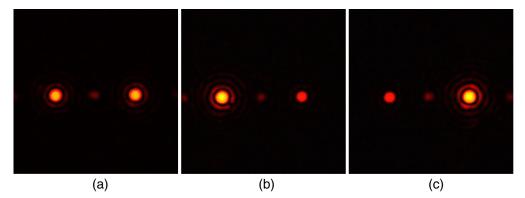
Finally, another possibility for getting rid of the DC term is to encode the lens function (L_2) in the SLM together with the phase pattern. This focuses the Fourier transform of the diffractve pattern while maintaining the collimated DC term, thus only contributing to some background noise.[17] Here however, we kept an external lens to perform the Fourier transform to clearly illustrate the fringing field effect characteristic of modern LCOS-SLMs as well as avoid additional functions for the multiplexed phase mask. The external glass lens has a focal length of 40 cm (Fig. 1). In the remaining experiments, we use the increased phase modulation depth technique to elliminate the DC term, as in Fig. 3(b).

Figure 5 shows the multiplexing of two outputs in which we vary the positions and patterns. In Fig. 5(a), the positions of the two outputs are different from Fig. 3, one being diffracted in the horizontal direction and the other in the vertical direction, corresponding to the situation illustrated in Fig. 2. Figure 5(b) illustrates how the two outputs can be made completely independent. Here one output additionally encodes a spiral phase generating a vortex beam of topological charge $\ell = 3$. Finally, Fig. 5(c) shows how we can superimpose the two outputs at the same location to produce their interference. In this case, the two outputs have opposite spiral phases with charges $+3$ and -3, so their interference shows six azimuthal lobes.

In all of these previous results, the random binary amplitude patterns had 50% of pixels with value 1 and the other 50% with value 0. This way the two complementary arrays have the same

Fig. 5 Experimental results of multiplexing two phase functions. (a) Result showing how the positions of the two beams can be changed arbitrarily. (b) Result with two different output beams. (c) Result for two oppositely charged outputs superimposed to produce their interference.

Fig. 6 Experimental results of multiplexing two phase functions. (a) Result for the two random patterns having the same number of pixels. (b) Result for the pattern for the left output having 75% of the pixels. (c) Result for the array for the left output having 25% of the pixels.
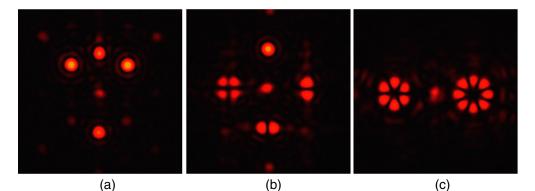
weight and the two output patterns are equally intense, as shown in Fig. 6(a). However, the intensity of each output can be easily weighted by simply changing the relative number of pixels in each pattern. Figure 6(b) shows the case in which the first pattern has 75% of the pixels and the second has 25%, and Fig. 6(c) shows the opposite case. Therefore, the relative intensities can be controlled at will simply by controlling the percentage of pixels assigned to each pattern. We recently made use of this property in a Fourier transform processor to control the two orthogonal polarization components of vector beams.[19]

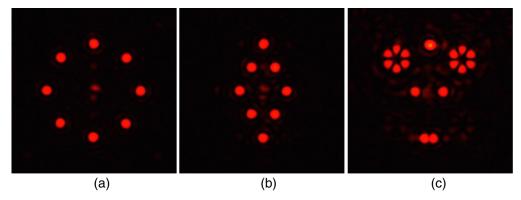Next we show results in which we increase the number of output patterns.

3 Increasing the Number of Output Patterns

The technique can be extended to add an arbitrary number of outputs simply by adding more random binary amplitude patterns. In this section, we demonstrate results with four and eight independent outputs. We keep the orthogonal random binary amplitude patterns labeled as A and a mentioned above (Fig. 2), and now create two other different orthogonal random patterns labeled B and b. We use these four binary 0-1 patterns to form four random binary amplitude arrays as AB, Ab, aB, and ab, where each case represents the product of the corresponding arrays [i.e., AB denotes $A(x,y)B(x,y)$, Ab denotes $A(x,y)b(x,y)$, etc.]. Again, these four arrays are orthogonal, each one now having $N^2/4$ pixels.

Some beautiful output patterns can be formed, as shown in Fig. 7, where each of the four binary amplitude patterns is multiplied by a different phase function and added to build the final multiplexed phase mask. In Fig. 7(a), four blazed diffraction gratings are multiplexed diffracting

Fig. 7 Experimental results of multiplexing four phase functions. (a) Result with four blazed gratings at different locations. (b) Result for the phase of Hermite–Gauss modes HG_{00}, HG_{10}, HG_{01}, and HG_{11} being added to blazed gratings in vertical and horizontal directions. (c) Result for the superposition of LG modes with charges of ± 3 on the left order and ± 4 on the right order.

Fig. 8 Experimental results of multiplexing eight phase functions. (a) Result for the location of the output dots forming a circle. (b) Result for the location of the output dots forming a rhomb. (c) Result showing an attempt to make a face having three regular spots, the superposition of positive and negative LG_{03} modes to create the "eyes" and the addition of the HG_{01} mode to create the "mouth."

in different directions (two along the vertical direction and other two in the diagonal directions), thus creating four bright spots. In Fig. 7(b), in addition to the four blazed gratings in the vertical and horizontal directions, we added the phases of Hermite–Gauss modes HG_{10}, HG_{01}, and HG_{11}. Therefore, the corresponding orders show their characteristic intensity patterns. Finally, Fig. 7(c) shows the result of using the four multiplexed functions to create two superpositions of Laguerre–Gauss modes: namely, LG_{03} and LG_{0-3} on the left order, and LG_{04} and LG_{0-4} on the right order, featuring six and eight azimuthal lobes, respectively.

Finally, we present results in which we multiplex eight different output beams. We create two additional random binary amplitude patterns now labeled C and c. Eight orthogonal random patterns are obtained as ABC, ABc, AbC, Abc, aBC, aBc, abC, and abc. Now the number of pixels in each pattern is reduced to $N^2/8$.

Figure 8 shows the corresponding experimental results. Figure 8(a) shows a case in which the positions of the eight outputs form a circular pattern. Note that all images in this work have been taken with the same level of input intensity. Therefore, the eight focused spots in Fig. 8(a) are now four times weaker than the two spots in Fig. 6(a). In Fig. 8(b), the positions of the spots are set to form a rhomb. Finally in Fig. 8(c), we attempted to form the pattern of a face. Four of the orders were used to form the "eyes" by superimposing the phases of the LG_{03} and LG_{0-3} modes, following the result in Fig. 7(c). The other four orders were used to make the rest of the "face." Finally, the light in the bottom corresponds to a single spot where the phase of the HG_{10} mode was added to mimic the "mouth."

4 Conclusions

In summary, we investigated the application of the random multiplexing technique of multiple phase masks in a liquid-crystal SLM. This random approach represents a very simple way of multiplexing different functions onto a single phase-only mask, avoiding the use of iterative algorithms or encoding complex valued functions. We showed that the large number of pixels available in modern LCOS-SLMs is useful for increasing the number of multiplexed masks. We showed experimental results with two, four, and eight multiplexed phase functions, showing a good reproduction of the individual functions.

However, the technique can be limited by the fringing field effect present in these SLM devices, which causes a significant DC term. We have shown that this DC term can be eliminated by increasing the phase modulation depth with which the phase patterns are displayed or by increasing the size of the random dots in the binary amplitude patterns.

We presented results obtained with a Hamamatsu LCOS-SLM with 792×600 pixels of $20~\mu$m pixel size. Once the fringing field effect was compensated, this SLM produced good results in the multiplexing technique. We also used an Exulus-HD1/M from Thorlabs with 1920×1080 pixels and $6.4~\mu$m pixel size. The experiments worked fairly well, but they were affected by a more significant DC term, as expected from the smaller pixel size in this SLM.

Finally, we point out that we only showed results with phase-only patterns. However, the same technique could be combined with different encoding techniques[20–22] that are useful for encoding amplitude information onto phase functions to achieve general multiplexed complex valued functions. We expect that this approach for multiplexing multiple patterns will have many applications.

Code, Data, and Materials Availability

Data underlying the results presented in this paper are not publicly available at this time but may be obtained from the authors upon reasonable request.

References

1. H. J. Caulfield, "Wavefront multiplexing by holography," *Appl. Opt.* **9**(5), 1218–1219 (1970).
2. J. A. Davis et al., "Multiplexed phase-encoded lenses written on spatial light modulators," *Opt. Lett.* **14**(9), 420–422 (1989).
3. C. Iemmi et al., "Depth of focus increase by multiplexing programmable diffractive lenses," *Opt. Express* **14**(22), 10207–10219 (2006).
4. R. L. Eriksen, V. R. Daria, and J. Glückstad, "Fully dynamic multiple-beam optical tweezers," *Opt. Express* **10**(14), 597–602 (2002).
5. J. Wang et al., "Terabit free-space data transmission employing orbital angular momentum multiplexing," *Nat. Photonics* **6**, 488–496 (2012).
6. S. Shwartz, M. A. Golub, and S. Ruschin, "Computer-generated holograms for fiber optical communication with spatial-division multiplexing," *Appl. Opt.* **56**(1) A31–A40 (2017).
7. C. Rosales-Guzman et al., "Multiplexing 200 spatial modes with a single hologram," *J. Opt.* **19**(11), 113501 (2017).
8. A. Martínez, I. Moreno, and M. M. Sánchez-López, "Comparative analysis of time and spatially multiplexed diffractive optical elements in a ferroelectric liquid crystal display," *Jpn. J. Appl. Phys.* **47**(3), 1589–1594 (2008).
9. J. A. Davis and D. M. Cottrell, "Random mask encoding of multiplexed phase-only and binary phase-only filters," *Opt. Lett.* **19**(7), 496–498 (1994).
10. J. A. Davis et al., "Four-plane space-variant Fresnel-transform optical processor with a random phase encoder," *Appl. Opt.* **35**(20), 3819–3828 (1996).
11. F. Xiao and L. Kong, "Optical multi-beam forming method based on a liquid crystal optical phased array," *Appl. Opt.* **56**(36), 9854–9861 (2017).

12. M. Szatkowski et al., "Generation of composite vortex beams by independent spatial light modulator pixel addressing," *Opt. Commun.* **463**, 125341 (2020).

13. Z. Zhang, Z. You, and D. Chu, "Fundamentals of phase-only liquid crystal on silicon (LCOS) devices," *Light: Sci. Appl.* **3**, e213 (2014).

14. R. Li et al., "Generating large topological charge Laguerre–Gaussian beam based on 4K phase-only spatial light modulator," *Chin. Opt. Lett.* **20**(12), 120501 (2022).

15. C. Lingel, T. Haist, and W. Osten, "Optimizing the diffraction efficiency of SLM-based holography with respect to the fringing field effect," *Appl. Opt.* **52**(28), 6877–6883 (2013).

16. I. Moreno et al., "Simple method to evaluate the pixel crosstalk caused by fringing field effect in liquid-crystal spatial light modulators," *J. Eur. Opt. Soc. Rapid Pub.* **17**, 27 (2021).

17. J. A. Davis et al., "Encoding complex amplitude information onto phase-only diffractive optical elements using binary phase Nyquist gratings," *OSA Contin.* **4**(3), 896 (2021).

18. S. Moser, M. Ritsch-Marte, and G. Thalhammer, "Model-based compensation of pixel crosstalk in liquid crystal spatial light modulators," *Opt. Express* **27**(18), 25046–25063 (2019).

19. J. A. Davis et al., "Vector beams generated with a Fourier transform processor with geometric phase grating," *Opt. Eng.* **62**(1), 013104 (2023).

20. J. A. Davis et al., "Encoding amplitude information onto phase-only filters," *Appl. Opt.* **38**(23), 5004–5013, (1999).

21. S. N. Khonina, V. V. Kotlyar, and V. A. Soifer, "Techniques for encoding composite diffractive optical elements, " *Proc. SPIE* **5036**, 493–498 (2003).

22. V. Arrizon, "Optimum on-axis computer-generated hologram encoded into low-resolution phase-modulation devices," *Opt. Lett.* **28**(24), 2521–2523 (2003).

Jeffrey A. Davis received his BS degree in physics from Rensselaer Polytechnic Institute and his PhD from Cornell University. He is a professor of physics at San Diego State University, where he leads the electro-optics program. His research interests include optical pattern recognition, spatial light modulators, and programmable diffractive optical elements. He is coauthor of more than 200 publications in peer-reviewed journals. He is a fellow of SPIE and of Optica (former OSA).

Ignacio Moreno is professor of optics at University Miguel Hernández (UMH). He graduated in physics and received his PhD at Autonomous University of Barcelona (UAB). After two years at University of Valencia, he joined UMH. His research is centered in the field of spatial light modulators for diffractive and polarization optics. He is fellow of SPIE and Optica. He was president of SEDOPTICA (2017–2020) and he is now secretary of the European Optical Society (EOS).

Shang Gao is a PhD student at University Miguel Hernández (UMH). She received her bachelor's degree in physics from the University of Yanbian in China, and her master's degree in photonics engineering from UC3M in Madrid. Now, she is working on her PhD centered in the field of structured light.

María del Mar Sánchez-López is professor of applied physics at UMH. She graduated in physics and received her PhD at UAB. After a post-doc with INFM, Salerno (Italy), she joined UMH. Her research activity is centered on structured light and liquid-crystal devices. She is a senior member of SPIE. She is member of Real Sociedad Española de Física, where she served as president of its Local Section of Alicante (2017–2021).

Don M. Cottrell received his BS and PhD degrees from the University of Washington. He is an emeritus professor of physics at San Diego State University. His research interests include the computer construction of synthetic holograms and the computer program used in this research. He also conducts theoretical studies in general relativity and particle physics involving differential geometry and supersymmetry.